ISSN 1069-3513, Izvestiya, Physics of the Solid Earth, 2020, Vol. 56, No. 6, pp. 911–919. © Pleiades Publishing, Ltd., 2020.

Condition of Occurrence of Large Man-made Earthquakes in the Zone of Oil Production, Oklahoma

Inessa Vorobieva[a], *, Peter Shebalin[a], **, and Clément Narteau[b], ***

[a] *Institute of Earthquake Prediction Theory and Mathematical Geophysics, Moscow, 117997 Russia*

[b] *Université de Paris, Institut de physique du globe de Paris, CNRS, Paris, F-75005 France*

**e-mail: vorobiev@mitp.ru,*

***e-mail: p.n.shebalin@gmail.com*

****e-mail: narteau@ipgp.fr*

Abstract—Man-made seismicity is a response of the brittle crust to fluid injection at depth and to the subsequent increase in pore-pressure and stress field perturbations. In Oklahoma, where the sharp increase in earthquake rate correlates with injection operations, we show that the earthquake-size distribution can differ significantly on the volume of injected fluid. The size distribution of $M < 3.5$ earthquakes exhibits a near-constant slope b, while significant variation of b-values (from $b \approx 1$ to $b > 2$) may be documented for larger magnitude ranges. This change shows statistically significant positive dependence on injection activity. In addition, largest events occur at the border of the injection area at some distance from massive injection, and in the periods of steady injection rate. These observations suggest that a deficit of large induced earthquakes under conditions of high injection rate can be accompanied by an overall increase of natural seismicity along pre-existing faults in the surrounding volume, where large events are more likely to be triggered over longer space-time scales.

Keywords: man-made seismicity, triggered seismicity, Oklahoma, fluid injection, b-value, band-limited analysis

DOI: 10.1134/S1069351320060130

INTRODUCTION

Fluid injection at depth can produce an increase in earthquake activity under the combined effect of pore-pressure changes and stress field perturbations (Davis and Frohlich, 1993; Ellsworth, 2013; Rubinstein and Mahani, 2015; Adushkin and Turuntaev, 2015). First, the frictional strength of faults decreases significantly as the pore pressure in excess to lithostatic pressure reduces the effective normal stress and simplifies beginning of slip. This mechanism supposes a direct hydrological connection between injection wells and faults. Second, deep fluid injection can modify the stress field and the loading conditions in the surrounding rock volume, even in zones with no direct change in pore pressure. Physical mechanism of these earthquakes meets most of the characteristics of the seismicity associated with active tectonic zones. These two mechanisms can initiate seismic ruptures, which are commonly referred to as induced or triggered earthquakes (Adushkin and Turuntaev, 2015). These two types of events are difficult to distinguish from one another nearby injection wells and a major question is to determine if they have a statistical signature in earthquake catalogs.

Oklahoma have experienced a dramatic increase in earthquake rate over the last decade following fluid injection operations associated with the development of oil and gas production (Walsh and Zoback, 2015). Located in the neighborhood of injection wells (Fig. 1a), seismic activity includes $M \geq 5.0$ earthquakes (Table 1) occurring on near-vertical strike-slip faults in the shallow Precambrian basement at 4–7 km depths (Grandin et al., 2017; Schoenball and Ellsworth, 2017b). These earthquakes are large enough to cause significant damage at the surface, highlighting the importance of seismic hazard assessment for the entire area (Ellsworth et al., 2015).

For natural or induced seismicity, all probabilistic seismic-hazard methods include an analysis of earthquake-size distribution, which is known to follow the Gutenberg-Richter law (GR):

$$\log_{10} N = a - bM, \quad (1)$$

where N is the number of earthquakes with a magnitude $m \geq M$, and a is the earthquake productivity, which depends on the space-time window of observation. The slope b is the scaling parameter, which gives the occurrence rate of large and rare events with respect to the occurrence rate of smaller and more fre-

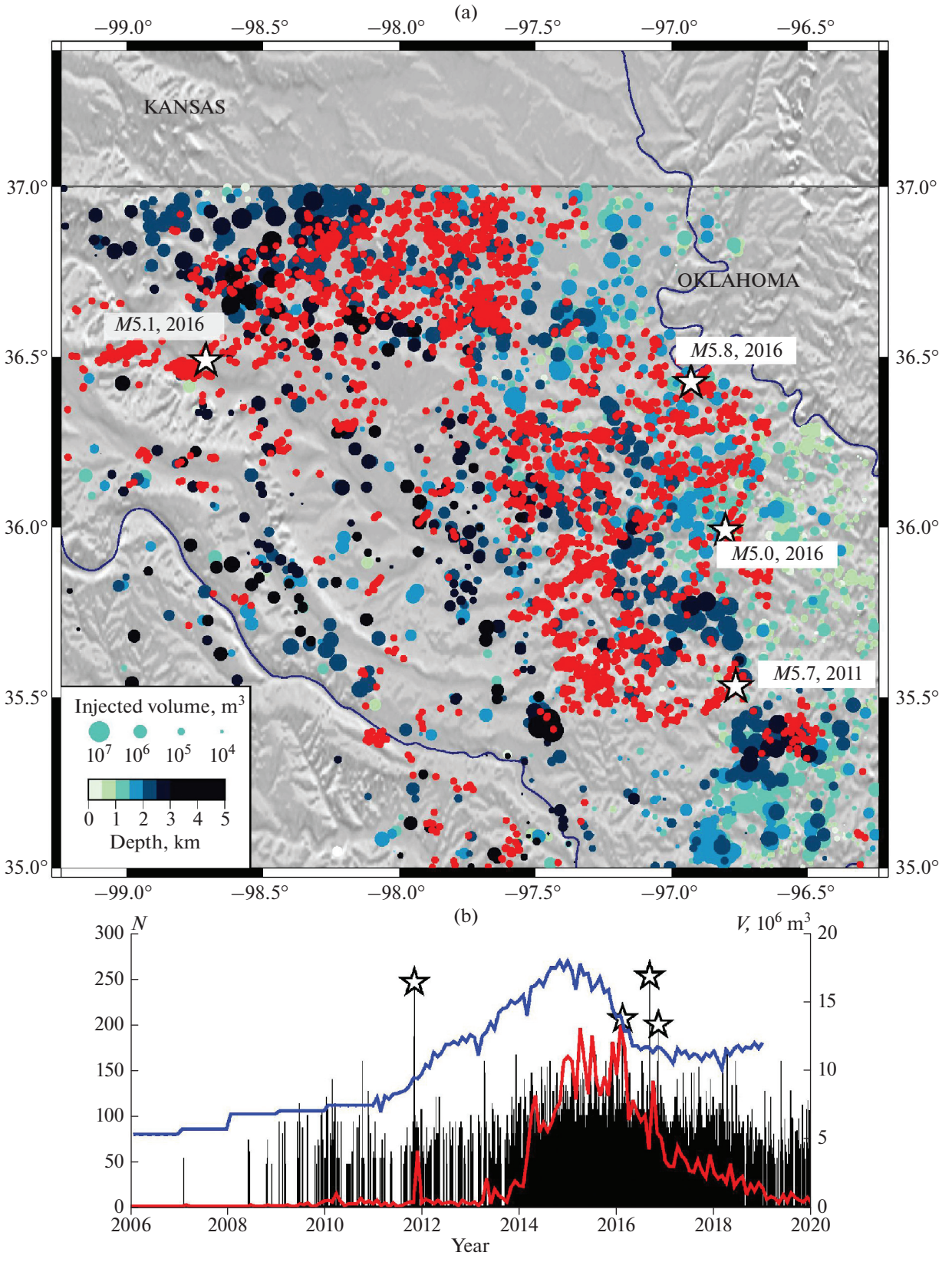

Fig. 1. Seismicity and fluid injection in Oklahoma. (a) Map of earthquakes and injection wells: $M \geq 2.7$ earthquakes in the ANSS catalog (red dots); $M \geq 5.0$ earthquakes (stars); injection depth and injected volume from 2006 to 2018 (filled circles). (b) Earthquake sequence (black bars); monthly number of $M \geq 2.7$ earthquakes (red line) and monthly volume of fluid injected (blue line) with respect to time. The 4 largest earthquakes shown in (a) give the magnitude scale.

Table 1. Large earthquakes in Oklahoma

Earthquake	Date	Epicenter lat°, lon°		Depth, km	Magnitude
Prague	2011.11.6	35.53	–96.77	5.20	5.7
Fairview	2016.2.13	36.49	–98.71	8.31	5.1
Pawnee	2016.9.3	36.43	–96.93	5.56	5.8
Cushing	2016.11.7	35.99	–96.80	4.43	5.0

quent earthquakes. Reported b—values are usually close to 1 along active tectonic structures, but also in zones of induced seismicity and laboratory rock mechanics experiments (Wyss et al., 2004; Scholz et al., 1986; Dinske and Shapiro, 2013). Nevertheless, there is not an universal b – value and its variations are increasingly studied to infer changes in stress conditions (Schorlemmer et al., 2005; Narteau et al., 2009; Rivière et al., 2018). It has also been suggested that the earthquake-size distribution may deviate from a single power-law model (Eq. 1). These deviations may result from finite size effects associated with structural properties (Romanovicz, 1992), or from aseismic deformation processes such as creep (Heimpel and Malin, 1998; Tormann et al., 2014; Vorobieva et al., 2016). In zones of induced seismicity, similar deviations have been observed and may be ascribed to the same underlying mechanisms (Shapiro et al., 2011, 2013). In this case, finite size effect can arise from the relative confinement of the stimulated rock volume; aseismic processes can be associated with high fluid pressure close to the injection wells.

Here we explore the spatio-temporal properties of the earthquake-size distribution in Oklahoma with respect to injection activity using the band limited analysis of b values in different magnitude ranges. Then, we analyze the conditions under which large earthquakes may occur.

METHODS FOR JOINT ANALYSIS OF SEISMICITY AND FLUID INJECTION ACTIVITY

The location, the depth and the fluid injection volume of all wells shown in Fig. 1a are extracted from the database of the Oklahoma Corporation Commission (http://www.occeweb.com/og/ogdatafiles2.htm). This database provides annual injected volumes from 2006 to 2010 and monthly values until the end of 2018. It was shown in the number of studies (e.g. Hincks et al., 2018), that induced seismicity correlates with deep injection, so only the data from wells that reach 1.5 km, the average depth of the crystalline basement, are used in this study.

In the neighborhood of injection wells we select all earthquakes of the ANSS composite catalog (https://earthquake.usgs.gov/earthquakes/search/) since 2007 to 2019 in Oklahoma (Figs. 1a, 1b). The multiscale mapping of completeness magnitude developed by (Vorobieva et al., 2013) is used to compute the recording threshold M_c of this catalog over space. The method provides high-resolution map of M_c (Fig. 2). Considering the entire time period from January 2007 to December 2019, the catalog can be considered as complete for $M \geq 2.7$ earthquakes around most of the fluid injection sites. However, major earthquakes may also occur in zones where the catalog has a higher magnitude of completeness. For example, the epicenter of the 2011 M5.7 Prague earthquake is located in zone of $M_c \approx 3.0$.

Induced seismicity may occur over long distance according to hydrological connection at depth, within 10 km or more (Cornet et al., 2013). As a first approximation, we consider the model of point source diffusion to quantify the degree of influence of injected fluids at some distance from each well. For each earthquake we compute with respect to its location x and occurrence time t the "related volume" of injected fluid corresponding to a single well W which decreases with distance from the well according to the Gaussian law. Then we compute the total related injection fluid volume $V_E(x,t)$ from all wells:

$$V_E(x,t) = \sum 10^{-0.02r^2} \int_{t-1}^{t} V_W(t)\,dt; \qquad (2)$$

where r is the horizontal distance in km between the earthquake and well, and the sum is taken over all wells. We integrate the injected fluid volume V_W during one year before the earthquake that is an average time delay between injection and seismic response in Oklahoma (Hong et al., 2018). The constant 0.02 provides 100 times decrease of the fluid influence at 10 km from a well, which corresponds to a typical radius of triggered volume (Walsh and Zoback, 2015). In the same way we attribute the related injection fluid volume $V_E(x,t)$ to each earthquake. Using all the events with a magnitude $M \geq 2.7$ in the entire triggered seismicity area (Fig. 1a), we study the change in the earthquake-size distribution with respect to the activity of fluid injection.

The earthquake-size distributions are analyzed in two non-intersecting magnitude ranges, (2.7, 3.4) and (3.5, M_{max}). For both magnitude ranges, we compute the slopes $b_{M2.7}$ and $b_{M3.5}$ using the Gutenberg-Richter

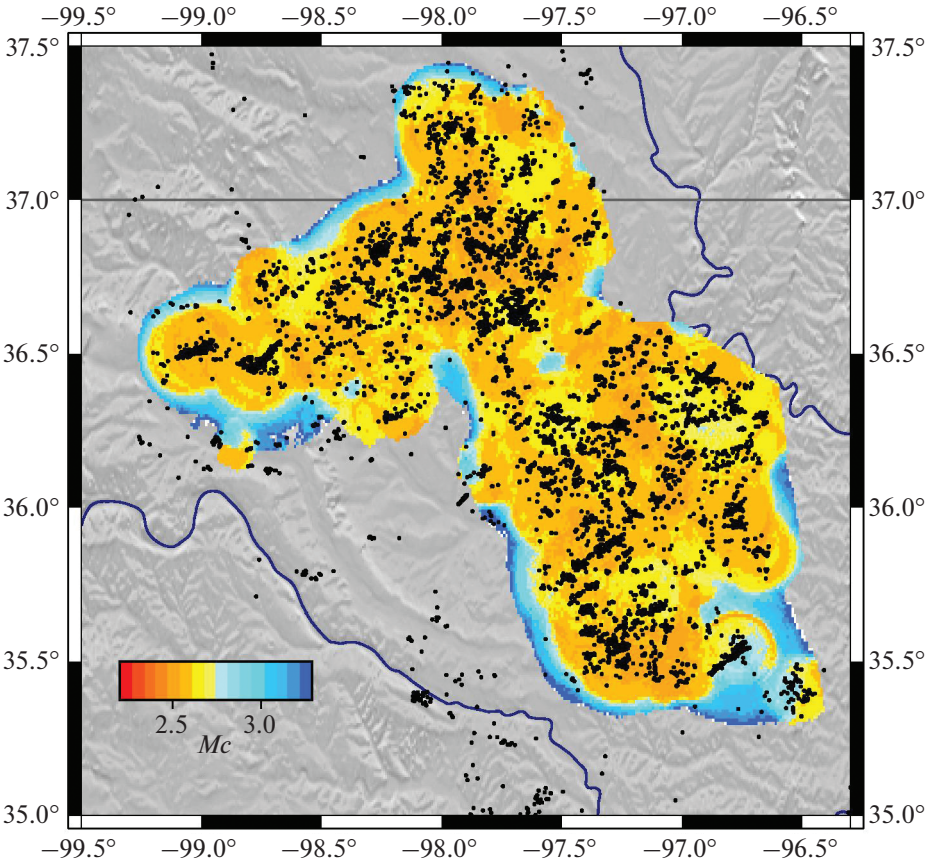

Fig. 2. Map of the completeness magnitude M_c in Oklahoma and southern Kansas using the multiscale method of (Vorobieva et al., 2013). $M \geq 2$ *:* 5 earthquakes in the ANSS catalog (black dots).

law and a maximum likelihood method for grouped data in truncated interval of magnitude (Bender, 1983). In contrast to the widely used Aki's method, the Bender's method provides an unbiased estimate of *b*-value in case of a short slope of the earthquake-size distribution (Marzocchi and Sandri, 2003). Throughout this article, this is described as a band-limited analysis of the *b*-value.

The band-limited analysis proposes a set of maximum likelihood formulas. Let N earthquakes be distributed in n magnitude bins of width Δm, and $\{k_1, k_2, ..., k_n\}$ be the number of events in the bins. The lower limit of the first bin corresponds to the minimum magnitude. The probability that an earthquake falls in the i-th bin writes p_i. Accordingly to the Gutenberg-Richter law

$$p_i = 10^{-b\Delta m} p_{i-1}, \quad (3)$$

where b is the slope of the earthquake size distribution. The value of p_1 is determined so that $\sum p_i = 1$. The likelihood function is

$$L = \frac{N!}{\prod_i k_i!} \prod_i p_i^{k_i}. \quad (4)$$

Setting the derivative $\partial \ln L/\partial b$ to zero, the maximum likelihood estimate of the *b*-value can be derived from

$$\frac{q}{1-q} - \frac{nq^n}{1-q^n} = \sum_{i=1}^{n} \frac{(i-1)k_i}{N}, \quad \text{where } q = 10^{-b\Delta m}. \quad (5)$$

This equation is solved by iterative procedure. The initial *b*-value is equal to 1 and $q_0 = 10^{-\Delta m}$. Then,

$$q_{j+1} = \left(\frac{nq_j^n}{1-q_j^n} + \sum_{i=1}^{n} \frac{(i-1)k_i}{N} \right)(1-q_j). \quad (6)$$

The iterations stop when $|q_j - q_{j-1}| < \varepsilon$. The procedure converges fast for $q < 1$.

EARTHQUAKE-SIZE DISTRIBUTION, INJECTION RATE AND LARGE EARTHQUAKES

We analyze how fluid injection activity changes the occurrence of larger earthquakes. Using eq. 2 each earthquake is attributed a total related volume corre-

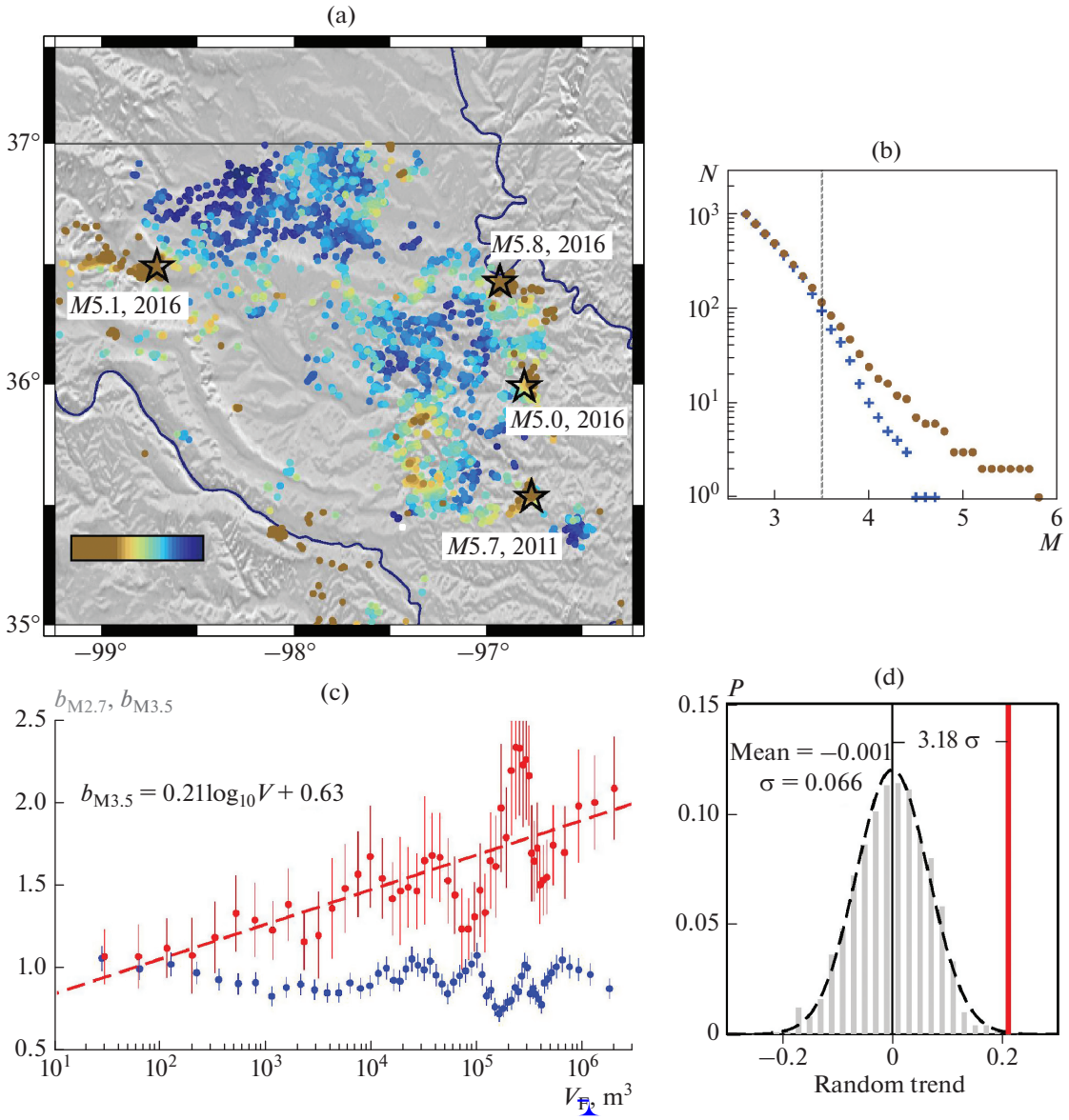

Fig. 3. Changes in earthquake-size distribution with respect to injection activity. (a) Map of the related injected fluid volume V_E attributed to $M \geq 2.7$ earthquakes. Stars show epicenters of large earthquakes (Table 1). (b) Earthquake-size distributions for 1000 events attributed the lowest (dots) and the highest (+) related fluid volume, respectively. (c), Slopes $b_{M3.5}$, and $b_{M2.7}$ of the earthquake-size distribution with respect to the related fluid volume in two magnitude ranges (2.7; 3.4) (blue dots) and (3.5; M_{max}) (red dots), respectively. Error bars are standard deviations obtained by bootstrap resampling, dashed red line shows a trend, the best linear fit between $b_{M3.5}$ and $\log_{10}V_E$. (d) Distribution of the slope of the best fit for 1000 semi-synthetic catalogs and its approximation by Gaussian distribution; the observed slope is shown by red bar.

sponding to all nearby wells. Marking epicenters by different colors according to this attribute (Fig. 3a), we may see a convolution of seismicity with related injection volumes in space and time. It is clearly seen that large earthquakes have occurred at locations of law related injection volume. The plot (Fig. 3b) shows earthquake size distributions for 1000 earthquakes attributed the smallest related injection volume and for 1000 earthquakes attributed the largest related volume V_E. The graphs match each other in the range of small magnitudes, while the slopes significantly differ for larger earthquakes.

Using the band-limited analysis and a sliding window algorithm, we calculate $b_{M3.5}$ and $b_{M2.7}$. We use constant sample size for $b_{M3.5}$, 50 events with $M \geq 3.5$, and the same interval of the related volumes for the corresponding $b_{M2.7}$-value. The uncertainties $\delta b_{M2.7}$ and $\delta b_{M3.5}$ are estimated as a standard deviation obtained from bootstrap resampling. Figure 3c shows that $b_{M2.7}$ keeps a steady value regardless of the injec-

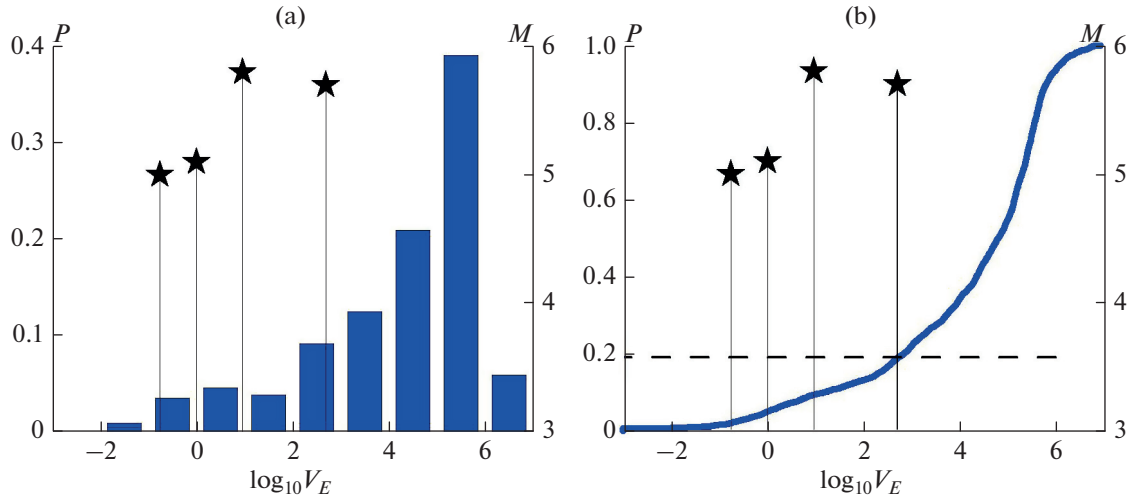

Fig. 4. Distribution of the Oklahoma earthquakes with $M \geq 2.7$ by related volume; large earthquakes $M \geq 5.0$ are shown by stars. (a) Histogram shows growth of earthquake number with respect of injection activity. (b) The probability of earthquake occurrence depending on related volume. All earthquakes with $M \geq 2.7$ fall to lower 20% quintile.

tion activity. On the contrary, the $b_{M3.5}$ -value shows a positive correlation with the injected fluid volume. At low related volumes, the slope $b_{M3.5} \approx 1.0 - 1.2$, that is a typical value for natural seismicity, and at maximum related volumes $b_{M3.5}$ exceeds 2. Dashed line in Fig. 3c shows a trend, the slope of the best linear fit between $b_{M3.5}$ and $\log_{10}(V_E)$. To check a statistical significance of this correlation we generated 1000 semi-synthetic catalogs using earthquakes with $M \geq 3.5$: we keep related volumes, but randomly mix magnitudes. Then, for each catalog, we determine the best linear fit like shown in Fig. 3c. The slope of the best linear fit is normally distributed with zero mean and standard deviation 0.066 (Fig. 2d). The observed trend of 0.21 differs from the mean random trend by more than 3 standard deviations. Therefore, the increase of the $b_{M3.5}$-value with the increase of the injected fluid volume is statistically significant at 0.999 level.

This result suggests that injection operations can affect the shape of earthquake size distribution of induced seismicity: we observe a deficit of large events under conditions of high injection rate. Although the deep fluid injection undoubtedly causes an overall increase of seismicity, and the number of earthquakes correlates with the related fluid volumes (Fig. 3a), surprisingly, the largest earthquakes occur essentially in space-time regions of low injection activity. All four large earthquakes (Table 1) with $M \geq 5.0$ fall to lower 20% quintile in the distribution of the related volumes (Fig. 4b). The probability to have such outcome by chance is as law as $p = 0.2^4 = 0.0016$.

In fact, all four major earthquakes have occurred at a distance of 15–20 km from the massive injection operations during one year before the earthquake, and in the periods of relatively steady injection rate (Fig. 5).

DISCUSSION AND CONCLUSION

Our statistical procedure has been developed to identify changes in earthquake activity depending on the proximity and intensity of the deep fluid injection. Applied to zones of deep fluid injection in Oklahoma, our analysis shows that the shape of earthquake-size distribution can change significantly. In areas of high injection rates we observe anomaly steep slope $b_{M3.5} \approx 2.0$ that provides unambiguous evidence for decreased probability of large earthquakes in the vicinity of the massive injection, in spite of the highest rate of seismicity. Away from injection wells, a similar increase in seismic activity may be observed, but with a normal slope $b_{M3.5} \approx 1.0$–1.5.

Such a difference in earthquake-size distributions may be related to the nature of the stress perturbation in these different regions, either by the increase of pore pressure or by an elastic stress transfer. Following fluid injection and the slow reactivation of faults, Schoenball and Ellsworth (2017a) observe that the resulting seismicity in Oklahoma meets most of the characteristics of the seismicity associated with active tectonic zones. Here, we find that induced and triggered events in Oklahoma have distinct signatures in earthquake-size distributions: Earthquakes, triggered by static stress transfer, may exhibit a power-law regime and occurrence of strong shocks, typical for natural tectonic seismicity. Barbour et al. (2017), Chen et al. (2017) note the significant role of elastic stress transfer leading to the Mw5.8 Pawnee earthquake. Earthquakes induced by pore pressure perturbations are likely to display a deficit of large events.

Similar distributions have been also documented along active tectonic faults and in volcanic areas where the role of fluids or inelastic deformations cannot be

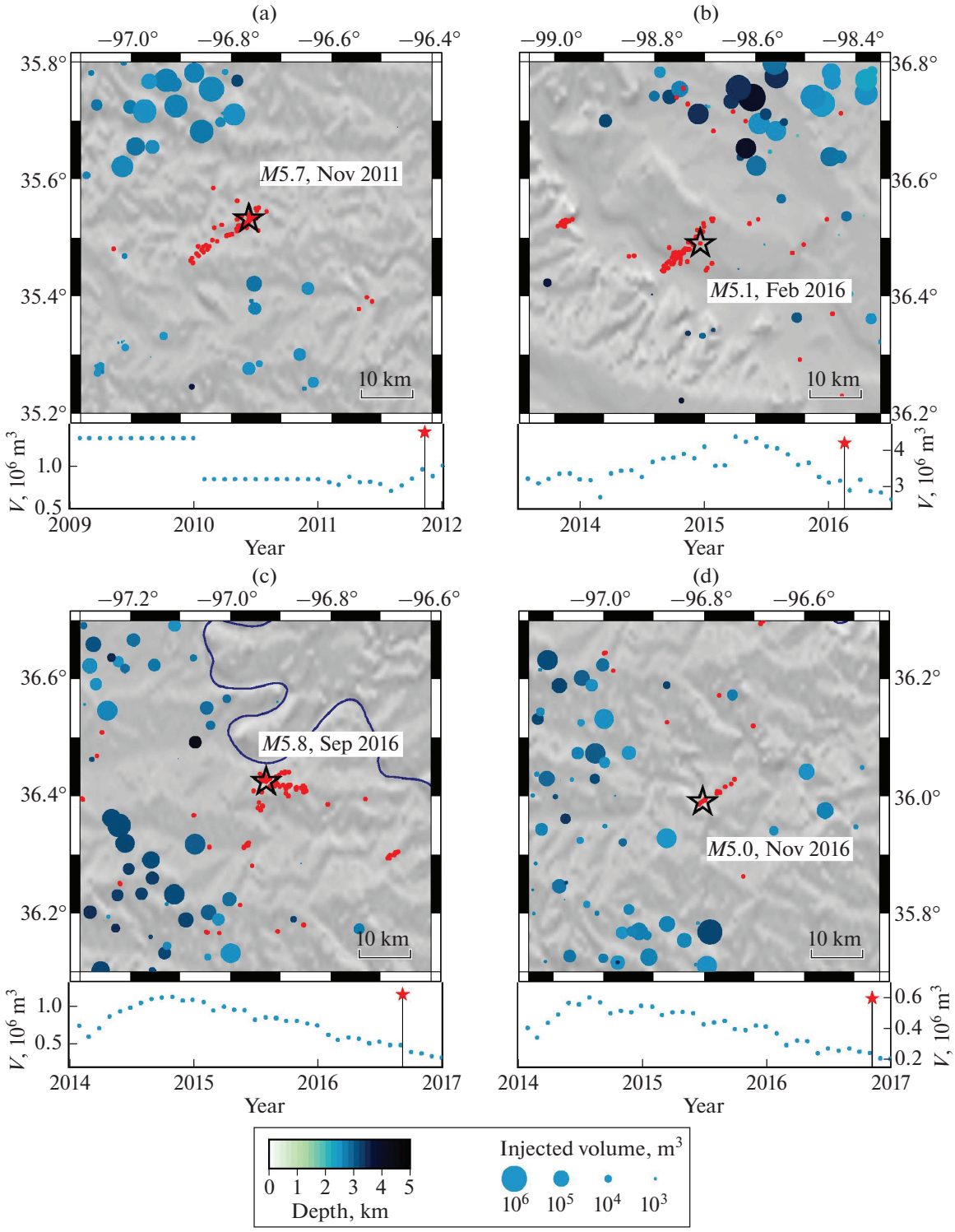

Fig. 5. Local injection activity before largest earthquakes in Oklahoma. (a) Prague, 2011, *M*5.7, (b), Fairview, February 2016, *M*5.1, (c), Pawnee, September 2016, *M*5.8, and (~~e~~), Cushing, November 2016, *M*5.0. Maps show injection during one year before large earthquake: Blue circles show locations of active wells and injected volumes. Three months aftershocks (red dots) delineate source zones of large earthquakes shown by stars. Plots exhibit variation of the monthly volume for wells shown in the maps during 3 years.

neglected (Vorobieva et al., 2016, 2019, Tormann et al., 2014). Thus, the effect of anthropogenic perturbation on seismicity can be used to investigate the role of fluids in the man-made and natural earthquake process by taking advantage of known forcing conditions.

We interpret the changes in earthquake-size distributions observed in Oklahoma as a deficit of large events accompanying the overall increase in earthquake rate. This is supported by both, the constant *b*-values in smaller magnitude ranges, and the positive dependence of *b*-values on injection rate in higher magnitude ranges. Along creeping fault segments, Vorobieva et al. (2016) associate such a deficit of large earthquakes with high rate of creep promoting stress release at small length scale, and hindering the propagation of seismic ruptures. In zones of oil and gas production, injection activity under conditions of low deformation rate, the transient forcing and the relative confinement of the fluid is more likely to be responsible for the deficit of large events. In addition, the activated fault length distribution has a typical value of 1 km (Schoenball and Ellsworth, 2017a), which corresponds to the magnitude $M \approx 3.5–4.0$; this supports a decreased probability of earthquakes with $M > 4$.

Such a finite volume effect has been addressed and modeled by Shapiro et al. (2013), who propose theoretical earthquake-size distributions that could naturally explain a deficit of large event. In this model, the observed positive dependence of $b_{M3.5}$ slope on the injected volume may be explained by overlapping of stimulated volumes and the density of injection wells in Oklahoma.

Although a decrease of injection activity in 2015 led to a decrease of seismicity rate (Fig. 1b), three earthquakes with magnitude $M \geq 5$ occurred in 2016, and the future seismic hazard remains uncertain. A number of models proposed for seismic hazard assessment predicts the rate of seismicity with respect of injection volume and depth (Hincks et al., 2018) variation in the injection rate (Barbour et al., 2017), stress state of pre-existing basement faults (Langenbruch et al., 2018; Johann et al., 2018), but all these models suppose a constant *b*-value. Indeed, the distribution of small earthquakes does not show significant variations, while changes in slope of the earthquake-size distribution for moderate events could be relevant to seismic hazard assessments, especially in regions of intense injection activity such as Oklahoma. While zones of high injection rate characterized by high seismicity rate but large *b* value remain less prone to large earthquakes, the surrounding areas may present a highest hazard of large triggered events due to the overall increase in seismicity level. Our results suggest that local forecast in the regions of intensive oil and gas production should account for spatial and temporal heterogeneity in earthquake statistics, which may be derived from injection rate data.

REFERENCES

Adushkin, V.V. and Turuntaev, S.B., *Tekhnogennaya seismichnost'–indutsirovannaya i triggernaya* (Man-Made Seismicity: Induced and Triggered), Moscow: IDG RAN, 2015.

Barbour, A., Norbeck, J.H., and Rubinstein, J.L., The effects of varying injection rates in Osage county, Oklahoma, on the 2016 M_w 5.8 Pawnee earthquake, *Seismol. Res. Lett.*, 2017, vol. 88, no. 4, pp. 1040–1053. https://doi.org/10.1785/0220170003

Bender, B., Maximum likelihood estimation of *b*-values for magnitude grouped data, *Bull. Seismol. Soc. Am.*, 1983, vol. 73, no. 3, pp. 831–851.

Chen, X., N. Nakata, C. Pennington, J. Haffener, J.C., Chang, X. He, Z. Zhan, S. Ni, and J. I. Walter, The Pawnee earthquake as a result of the interplay among injection, faults and foreshocks, *Sci. Rep.*, 2017, vol. 7, paper ID 4945. https://doi.org/10.1038/s41598-017-04992-z

Cornet, F., Seismic and aseismic motions generated by large scale fluid injections in a deep granite massif, *Proc. 47th US Rock Mechanics/Geomechanics Symposium*, San Francisco, 2013, New York: Curran Associates, 2013, vol. 2, pp. 987–994.

Davis, S.D. and Frohlich, C., Did (or will) fluid injection cause earthquakes?-criteria for a rational assessment, *Seismol. Res. Lett.*, 1993, vol. 64, nos. 3–4, pp. 207–224.

Dinske, C. and Shapiro, S.A., Seismotectonic state of reservoirs inferred from magnitude distributions of fluid-induced seismicity, *J. Seismol.*, 2013, vol. 17, no. 1, pp. 13–25. https://doi.org/10.1007/s10950-012-9292-9

Ellsworth, L.E., Injection-induced earthquakes, *Science*, 2013, vol. 341, no. 6142, pp. 1225,942-1–1225,942-7. https://doi.org/10.1126/science.1225942

Ellsworth, W.L., Llenos, A.L., McGarr, A.F., Michael, A.J., Rubinstein, J.L., Mueller, C.S., Petersen, M.D., and Calais, E., Increasing seismicity in the U.S. midcontinent: Implications for earthquake hazard, *Leading Edge*, 2015, vol. 34, no. 6, pp. 618–626.

Grandin, R., Vallée, M., and Lacassin, R., Rupture process of the M_w 5.7 Pawnee, Oklahoma, earthquake from Sentinel-1 InSAR and seismological data, *Seismol. Res. Lett.*, 2017, vol. 88, no. 3, pp. 1–11.

Heimpel, M. and Malin, P., Aseismic slip in earthquake nucleation and self-similarity: evidence from Parkfield, California, *Earth Planet. Sci. Lett.*, 1998, vol. 157, no. 3, pp. 249–254.

Hincks, T., Aspinall, W., Cooke, R., and Gernon, T., Oklahoma's induced seismicity strongly linked to wastewater injection depth, *Science*, 2018, vol. 359, no. 6381, pp. 1251–1255. https://doi.org/10.1126/science.aap7911

Hong, Z., Moreno, H.A., and Hong, Y., Spatiotemporal assessment of induced seismicity in Oklahoma: Foreseeable fewer earthquakes for sustainable oil and gas extraction?, *Geosciences*, 2018, vol. 8, no. 436, pp. 1–15. https://doi.org/10.3390/geosciences8120436

Johann, L., Shapiro, S.A., and Dinske, C., The surge of earthquakes in Central Oklahoma has features of reservoir-induced seismicity, *Sci. Rep.*, 2018, vol. 8, no. 1, paper ID 11505. https://doi.org/10.1038/s41598-018-29883-9

Langenbruch, C., Weingarten, M., and Zoback, M.D., Physics-based forecasting of man-made earthquake haz-

ards in Oklahoma and Kansas, *Nat. Commun.*, 2018, vol. 9, no. 1, Paper ID 3946.
https://doi.org/10.1038/s41467-018-06167-4

Marzocchi, W. and Sandri, L., A review and new insights on the estimation of the b-value and its uncertainty, *Ann. Geophys.*, 2003, vol. 46, no. 6, pp. 1271–1282.
https://doi.org/10.4401/ag-3472

Narteau, C., Byrdina, S., Shebalin, P., and Schorlemmer, D., Common dependence on stress for the two fundamental laws of statitical seismology, *Nature*, 2009, vol. 462, no. 3, pp. 642–645.
https://doi.org/10.1038/nature08553

Rivière, J., Lv, Z., Johnson, P., and Marone, C., Evolution of b-value during the seismic cycle: Insights from laboratory experiments on simulated faults, *Earth Planet. Sci. Lett.*, 2018, vol. 482, no. 7, pp. 407–413.

Romanowicz, B., Strike-slip earthquakes on quasi-vertical transcurrent faults: Inferences for general scaling relations, *Geophys. Res. Lett.*, 1992, vol. 19, no. 5, pp. 481–484.
https://doi.org/10.1029/92GL00265

Rubinstein, J.L., and Mahani, A.B., Myths and facts on wastewater injection, hydraulic fracturing, enhanced oil recovery, and induced seismicity, *Seismol. Res. Lett.*, 2015, vol. 86, no. 4, pp. 1060–1067.
https://doi.org/10.1785/0220150067

Schoenball, M., and Ellsworth, W.L., A systematic assessment of the spatiotemporal evolution of fault activation through induced seismicity in Oklahoma and southern Kansas, *J. Geophys. Res.*, 2017a, vol. 122, no. 12, pp. 10189–10206.
https://doi.org/10.1002/2017JB014850

Schoenball, M. and Ellsworth, W.L., Waveform-relocated earthquake catalog for Oklahoma and southern Kansas illuminates the regional fault network, *Seismol. Res. Lett.*, 2017b, vol. 88, no. 5, pp. 1252–1258.

Scholz, C., Aviles, C., and Wesnousky, S., Scaling differences between large intraplate and interplate earthquakes, *Bull. Seismol. Soc. Am.*, 1986, vol. 76, no. 1, pp. 65–70.

Schorlemmer, D., Wiemer, S., and Wyss, M., Variations in earthquake-size distribution across different stress regimes, *Nature*, 2005, vol. 437, no. 7058, pp. 539–542.

Shapiro, S.A., Krüeger, O.S., Dinske, C., and Langenbruch, C., Magnitudes of induced earthquakes and geometric scales of fluid-stimulated rock volumes, *Geophysics*, 2011, vol. 76, no. 6, pp. WC55–WC63.
https://doi.org/10.1190/GEO2010-0349.1

Shapiro, S.A., Krueger, O.S., and Dinske, C., Probability of inducing given-magnitude earthquakes by perturbing finite volumes of rocks, *J. Geophys. Res.: Solid Earth.*, 2013, vol. 118, no. 7, pp. 3557–3575.

Tormann, T., Wiemer, S., and Mignan, A., Systematic survey of high-resolution *b*-value imaging along Californian faults: inference on asperities, *J. Geophys. Res.: Solid Earth*, 2014, vol. 119, no. 3, pp. 2029–2054.
https://doi.org/10.1002/2013JB010867

Vorobieva, I., Narteau, C., Shebalin, P., Beauducel, F., Nercessian, A., Clourad, V., and Bouin, M.-P., Multiscale mapping of completeness magnitude of earthquake catalogs, *Bull. Seismol. Soc. Am.*, 2013, vol. 103, no. 4, pp. 2188–2202.
https://doi.org/10.1785/0120120132

Vorobieva, I., Shebalin, P., and Narteau, C., Break of slope in earthquake size distribution and creep rate along the San Andreas Fault system, *Geophys. Res. Lett.*, 2016, vol. 43, no. 13, pp. 6869–6875.
https://doi.org/10.1002/2016GL069636

Vorobieva I.A., Soloviev, A.A., and Shebalin, P.N., Mapping of interplate coupling in the Kamchatka subduction zone from variations in the earthquake size distribution, *Dokl. Earth Sci.*, 2019, vol. 484, no. 4, pp. 478–481.
https://doi.org/10.31857/S0869-56524844478-481

Walsh, F.R. III and Zoback, M., Oklahoma's recent earthquakes and saltwater disposal, *Sci. Adv.*, 2015, vol. 1, no. 5, Paper ID e1500195.
https://doi.org/10.1126/sciadv.1500195

Wyss, M., Sammis, C., Nadeau, R., and Wiemer, S., Fractal dimension and *b*-value on creeping and locked patches of the San-Andreas fault near Parkfield, California, *Bull. Seismol. Soc. Am.*, 2004, vol. 94, no. 2, pp. 410–421.

SPELL: 1. OK